Modeling and optimization of radiative cooling based thermoelectric generators

Bin Zhao [a, b], Gang Pei [a] *, Aaswath P. Raman [b] *

[a] *Department of Thermal Science and Energy Engineering, University of Science and Technology of China, Hefei 230027, China*

[b] *Department of Materials Science and Engineering, University of California, Los Angeles, Los Angeles, CA 90024, USA*

* Corresponding authors. E-mail address: aaswath@g.ucla.edu, peigang@ustc.edu.cn

Abstract

Generating power at night has recently stimulated interest in using the radiative cooling mechanism with thermoelectric generators (TEG). These low temperature and passive devices have been shown to generate electricity at night with no active input of heat needed. Here, we optimize both the geometry and operating conditions of radiative cooling driven thermoelectric (RC-TE) generators. We determine the optimal operating conditions, including maximum power point and maximum efficiency point, by developing a combined thermal and electrical model. Our results show that the optimal operating condition results in larger power output than was previously expected. Moreover, we show that maximum power density occurs when the area ratio between cooler and P or N element reaches an optimal value and can be improved to nearly 2.2 times larger than what has been achieved with commercial TEGs. Finally, we perform a parametric study that takes account of environmental and structural parameters to improve the performance of the RC-TE device, including enhancing heat transfer between the hot surface and ambient air, suppressing the cooling loss of the radiative cooler, and optimizing the geometry of individual thermocouples. In summary, our work identifies how to maximize the output of RC-TE devices, providing universal guidance for this passive power generation method.

Main text

Radiative cooling is a passive cooling technique that cool objects by radiating a fraction of the object's thermal radiation to the cold of outer space[1–3]. This technique takes advantage of an atmospheric transparency window in the long-wave infrared band from 8 to 13 μm. Recent progress in the field has led to the recognition of radiative cooling as an important technology for both energy efficiency and energy harvesting applications.

Radiative cooling was initially explored during the night[4–8] with a range of materials and surfaces developed for efficient nighttime radiative cooling, such as white[9] and black paint[10], silicon related coatings[4,5,11,12], and polyester materials[13,14]. Recently, passive sub-ambient cooling has been demonstrated by radiative cooling at daytime under sunlight[15], which was a milestone for the technology's development. These advancements were achieved with material innovations, including photonic structures[15,16], metamaterials[3,17], and artificial materials[18], which maximally reduce solar absorption of the radiative cooler and simultaneously enhance its thermal emissivity. These radiative cooling materials efficiently improve the performance of radiative cooling and enable its utilization for a range of potential applications that include energy-saving buildings[19–22], passive cooling of solar cells[23–26], and personal thermal managemnet[27–31].

More recently, the concept of power generation using radiative cooling and outgoing thermal radiation has drawn much attention. These studies include explorations of the fundamental limits of energy harvesting[32–34] and detailed solutions[35–39], such as using the negative illumination effect of the semiconductor photodiode[35] and thermoelectric generators[36]. Here, we focus on the topic of using radiative cooling and a thermoelectric generator (TEG) to generate electricity at night, which is both a practical approach to night-time power generation, and an unconventional use of thermoelectric generators relative to systems such as solar TEGs[40]. In this approach, the radiative cooling surface is applied as the cold side of the TEG, while the hot side of the TEG is heated by the ambient environment. Thus, a temperature difference is passively created and electricity can be generated by TEG. Raman et al.[36] experimentally demonstrated this concept by coupling the cold side of the TEG to a near-black surface that radiates thermal radiation to outer space and has its hot side heated by ambient air, achieving electricity generation to successfully light a LED. Similarly, recent efforts have also investigated all-day electricity generation using radiative cooling and TEGs[37–39,41]. While these reports are intriguing, comparatively less is known about the limits of performance of radiative cooling based thermoelectric (RC-TE) devices and what mechanisms exist to optimize performance.

Motivated by this consideration, Fan et al.[42] recently showed that with future improvements to the ZT of the thermoelectric generator, and improvements to spectral selectivity as well as insulation, power density could in theory be improved to larger than 2 $W \cdot m^{-2}$. However, the maximum power point of the TEG in this optimization occurs when the load electrical resistance equals the internal impedance of the TEG, which is consistent with the conclusions in prior work of TEGs[43,44]. This assumption neglects a key aspect of the radiative cooling driven TEG that is the focus of this paper: it is a low-temperature and entirely passive thermoelectric conversion case, with the hot and cold side's temperature, current, and voltage all closely coupled with the load electrical resistance. Thus, these parameters will change passively with different load electrical resistance input and the optimal condition for a radiatively-cooled TEG might not be predicted accurately using the previous conclusions. Although some scholars[45,46] have investigated this problem based on different detailed mathematical models, no studies have sought to optimize a radiative cooling driven thermoelectric conversion with a passively maintained low-temperature difference between the hot and cold side.

In this paper, we investigate the optimization of a RC-TE device to improve the operational performance of the RC-TE device using a combined thermal and electrical model. We consider a unit cell of universal TEG as shown in Fig. 1. A near-black infrared radiative cooler is applied as the cold surface of the TEG unit cell and is exposed to the sky directly. Ambient environment is selected to be the heat source of the TEG unit cell. Heat energy is extracted from ambient air to the hot surface of the TEG mainly by convection and conduction and is dissipated by radiative cooling at the cold surface. Several assumptions are proposed to simplify the mathematical description of the thermal and electrical analysis of the device, which is presented as follows: 1) The thermal transfer process is a steady-state condition, 2) The temperature of the hot surface and cooler is uniform since the cooler and hot surface are thermal conductive material with a thin thickness, 3) Only thermal conduction is considered for P and N elements, 4) Radiative heat transfer between cooler and hot surface is assumed to be negligible, and 5) The Seebeck coefficient, internal impedance, and thermal conductivity of P and N elements are assumed to be temperature-independent since the temperatures of hot and cold side change within a small range and the temperature difference between the hot and cold sides in the TEG is also very small. These assumptions are consistent with previously published works for radiative cooling and TEGs[15,18,24,42,43,46].

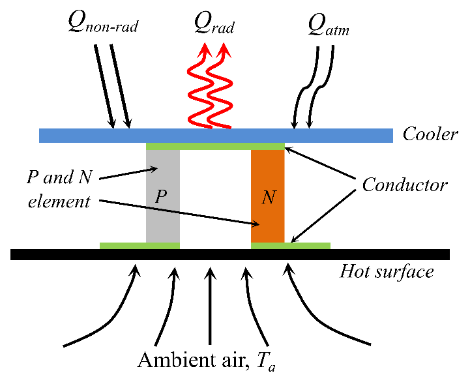

Fig. 1. Schematic of a unit cell of the RC-TE device. Q_{rad} is the thermal emissive power of the cooler, Q_{atm} is absorbed atmospheric thermal radiation power, $Q_{non\text{-}rad}$ is the power from ambient air to the cooler via conduction and convection.

Using the standard energy balance analysis for TEGs, the energy fluxes at the hot surface and cooler of the RC-TE device are determined by:

$$Q_h = S_{PN} T_h I + K_{PN}\left(T_h - T_c\right) - \frac{1}{2} I^2 R_{PN}, \quad (1)$$

$$Q_c = S_{PN} T_c I + K_{PN}\left(T_h - T_c\right) + \frac{1}{2} I^2 R_{PN}, \quad (2)$$

where Q is heat energy, I is current, T is temperature, S is Seebeck coefficient, K is thermal conductance, R is the electrical resistance, subscript $_h$ and $_c$ denote hot surface and cold surface, and subscript $_{PN}$ represents one PN thermocouple. Generally, S_{PN}, K_{PN}, and R_{PN} are closely related to the geometry of PN thermocouples and material properties of P and N elements[43,46,47]. The properties of P and N elements used in this paper are obtained from a commercial TEG module (TG12-4-01LS, Marlow Industries) and presented in Table 1 (this TEG was used and validated in the prior literature[46]).

Table 1. Properties of P and N TE elements.

Symbol	Physical meaning	Value
S_{PN}, μV·K^{-1}	Seebeck coefficient of one PN thermocouple	366
k_{PN}, W·m^{-1}·K^{-1}	Thermal conductivity of one PN thermocouple, $k_{PN}= k_P+ k_N$	3.64
A, mm^{-2}	Cross-section of P or N element	0.87
L, mm	Length of P or N element	1.6
ρ_{PN}, μΩ·m	Electrical resistance of one PN thermocouple, $\rho_{PN}= \rho_P+ \rho_N$	14.46

The output power of the TE unit cell can be obtained after introducing the load electrical resistance R_{load} using Eq. (3) and the electrical efficiency can be defined as the ratio of output power P_e and input heat flux Q_h.

$$P_e = I^2 R_{load} = \frac{S_{PN}^2 \left(T_h - T_c\right)^2}{\left(R_{PN} + R_{load}\right)^2} R_{load} \,. \tag{3}$$

Here, two area ratios $\gamma_{hot}= A_{hot}/A$ and $\gamma_{cold}= A_{cold}/A$ are defined to describe the area ratio relation between hot (cold) surface and cross-section of P or N element. According to the first law of thermodynamics, the heat energy obtained by the hot surface Q_h can be determined by the heat transfer process between the hot surface and ambient air. Besides, the heat energy dissipated by the cooler Q_c can also be represented by the net cooling power of the cooler. Thus,

$$Q_h = \gamma_{hot} A h_{hot} \left(T_a - T_h\right), \tag{4}$$

$$Q_c = Q_{rad} - Q_{atm} - Q_{non-rad} \,, \tag{5}$$

where h_{hot} is the effective heat transfer coefficient between the hot surface and local ambient air, T_a is ambient temperature, Q_{rad} is the thermal emissive power of the cooler, Q_{atm} is absorbed atmospheric thermal radiation power, $Q_{non\text{-}rad}$ is the power from ambient air to the cooler via conduction and convection. In general, Q_{rad}, Q_{atm}, and $Q_{non\text{-}rad}$ can be obtained from the following expressions:

$$Q_{rad} = \gamma_{cold} A \varepsilon_{cooler} \sigma T_h^4 , \tag{6}$$

$$Q_{atm} = \gamma_{cold} A \varepsilon_{cooler} \varepsilon_{atm} \sigma T_a^4 , \tag{7}$$

$$Q_{non-rad} = \gamma_{cold} A h_{cold} \left(T_a - T_c \right), \tag{8}$$

where σ is the Stefan-Boltzmann constant, h_{cold} is the effective heat transfer coefficient between the cold surface and local ambient air, ε_{cooler} is the emissivity of the cooler, ε_{atm} is the effective emissivity of the atmosphere and has previously been experimentally determined[48] to fit the following model: $\varepsilon_{atm} = 0.741 + 0.0062 \times (T_{dew} - 273.15)$, where T_{dew} is dew point temperature in degrees Kelvin.

Here, the optimal operation condition of the RC-TE device is investigated by scanning the load electrical resistance in the electrical model. During simulation, the emissivity of the radiative cooler is set to 0.95, which can be obtained from commonly available materials such as paints. Moreover, a testing condition is also set for simulation. Ambient temperature is assumed to be 303.15 K, dew point temperature is 287.92 K (corresponding to a 40% relative humidity), h_{hot} and h_{cold} are set as 7 $W \cdot m^{-2} \cdot K^{-1}$, and γ_{hot} is set as 250 (estimated from our previous experimental work[36]).

Identifying the maximum power point (MPP) of a TEG device is key to maximizing the electricity output and effectiveness of a TEG system. In previous models (referred to as the "power model" hereon), it was widely recognized that the MPP of the TEG device occurs when the load electrical resistance is equal to the internal impedance of the TEG device. However, in our analysis, the MPP is determined by scanning the load resistance in our theoretical model (referred to as "Load scan model" hereon) and a load ratio r is defined for the load scan process, which can be calculated using load resistance over internal impedance: $r = R_{load}/R_{PN}$.

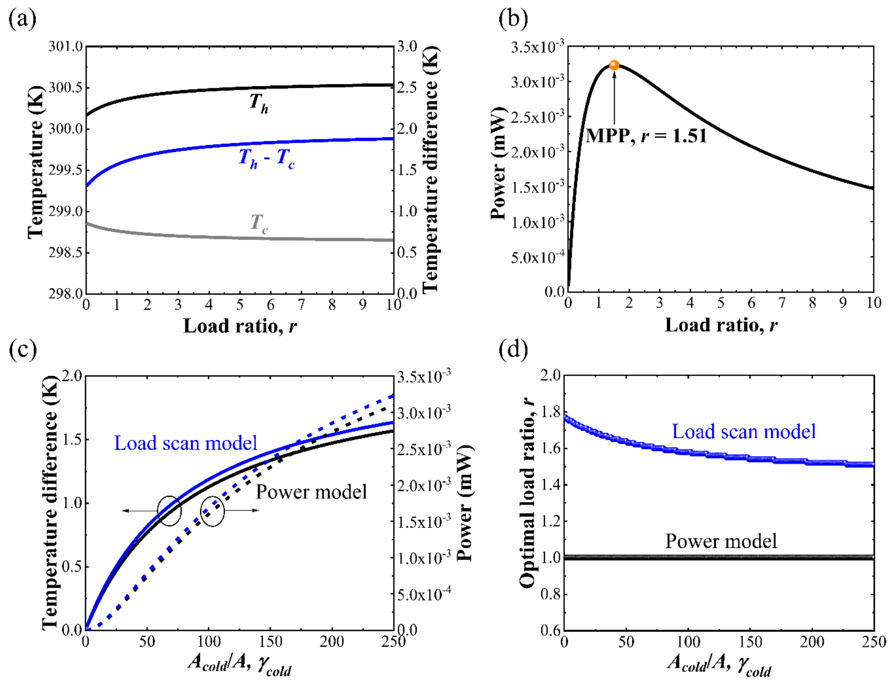

Fig. 2. (a)-(b) Temperature and power of the RC-TE device with different load ratios under $\gamma_{cold} = 250$. (c) temperature difference and power of the RC-TE device at MPP conditions under cold area ratio γ_{cold} from 1 to 250. (d) optimal load ratio at MMP conditions under cold area ratio γ_{cold} from 1 to 250.

Fig. 2(a) shows T_h and T_c change during the load resistance scanning process and the temperature difference between the hot and cold side of the RC-TE device increases with increasing load ratio. Thus, the MPP occurs when the load ratio equals to 1.51 (Fig. 2(b)), which is different from the MPP condition derived from the power model (where the load ratio would be 1). To compare the performance of the RC-TE device's MPP under two models, serials of MPPs (Fig. 2(c)) are obtained using both the Power model and the Load scan model for different γ_{cold}. It can be found the maximum power obtained by the Load scan model is greater than that predicted by the Power model, indicating that the traditional Power model is not appropriate to analyze and maximize the performance of this kind of fully-passive low-temperature RC-TE device. Moreover, the temperature difference and maximum power point gradually increase with increasing cold area ratio γ_{cold}, an easily implementable path to improve the performance of the RC-TE device. Notably, the optimal load ratios for the Load scan model and Power model are also quite different (Fig. 2(d)). The former one decreases gradually with increasing γ_{cold}, while the latter remains at one. Additionally, we develop a relationship for optimal load ratio of the Load scan model for MPP in this case, which is presented in Eq. (9):

$$r = 1.76515 - 3.69\times10^{-3}\gamma_{cold} + 2.63648\times10^{-5}\gamma_{cold}^{2} - 9.86644\times10^{-8}\gamma_{cold}^{3} + 1.43448\times10^{-10}\gamma_{cold}^{4} \quad (9)$$

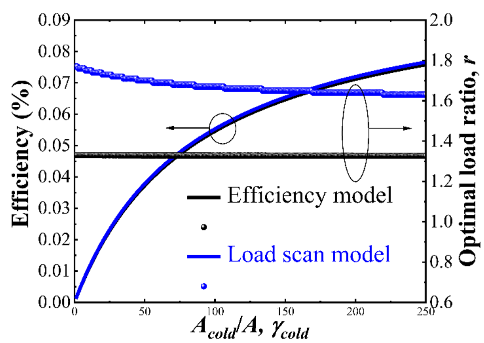

Fig. 3. maximum efficiency and corresponding load ratio of the RC-TE device at MEP conditions under cold side area ratio γ_{cold} from 1 to 250.

The maximum efficiency point (MEP) is another key indicator of TEG devices. According to the traditional model (referred to as "Efficiency model" hereon), MEP occurs when load resistance equals to $\sqrt{1+ZT_m}R_{PN}$, where ZT_m is a dimensionless figure of merit and T_m is the arithmetic mean temperature between T_h and T_c. Fig. 3 depicts the maximum efficiency and corresponding optimal load ratio at MEP conditions under different γ_{cold}. As can be seen, the optimal load ratio determined by the Load scan model is higher than that derived from Efficiency model and the estimated relationship with γ_{cold} for MEP in this case is shown in Eq. (10):

$$r = 1.76784 - 1.89\times10^{-3}\gamma_{cold} + 1.2715\times10^{-5}\gamma_{cold}^{2} - 4.44141\times10^{-8}\gamma_{cold}^{3} + 5.97181\times10^{-11}\gamma_{cold}^{4} \qquad (10)$$

Moreover, the optimal load ratio for the Load scan mode reduces gradually with increasing γ_{cold}, which is similar to the phenomenon described for MPP in Fig. 2(d). However, the maximum efficiency obtained by the Load scan model and Efficiency model is nearly consistent. The relative efficiency difference is only 1.1% even for $\gamma_{cold} = 250$, which is lower than that in MPP condition. The main reason is that the difference of optimal load ratio between the Load scan model and the Efficiency model is smaller than that between the Load scan model and the Power model. Thus, the MEP condition predicted by Efficiency model approaches that obtained by the Load scan model.

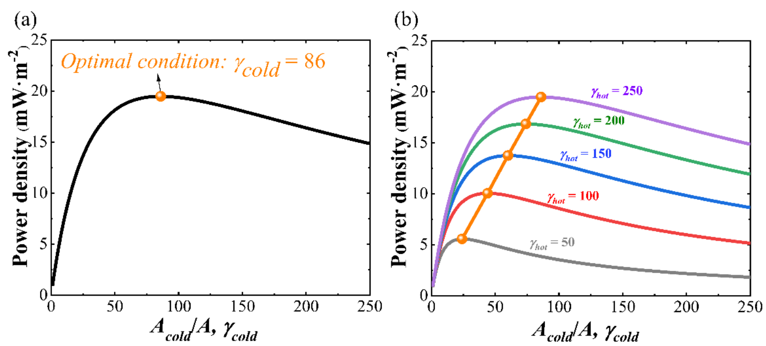

Fig. 4. (a) Power density of the RC-TE device under cold side area ratio γ_{cold} from 1 to 250 and hot side area γ_{hot} of 250. (b) power density of the RC-TE device under cold side area ratio γ_{cold} from 1 to 250 and different hot side area γ_{hot}.

The performance of the RC-TE device mainly relies on radiative cooling power which scales with the area of the radiative cooling surface. Thus, we proposed a power density parameter $P_{density}$ as the objective function to optimize the geometry of the TE module, which is defined as the ratio of output power and cold side area of TE module ($P_{density} = P_e/A_{cold}$). As shown in Fig. 4(a), we show that there exists a maximum power density point as radiative cooler area is increased. For the testing condition previously described, the maximum power density is approximately 19.5 $mW \cdot m^{-2}$ with an optimal cold side area ratio $\gamma_{cold} = 86$, which is nearly 2.2 times larger than that of commercial TEG (γ_{cold} is estimated as 8)[46]. This result is obtained under the condition that hot side area ratio $\gamma_{hot} = 250$. To investigate the effect of different hot side area ratio γ_{hot} on the maximum power density, a preliminary analysis is conducted and presented in Fig. 4(b). The maximum power density increases almost linearly with increasing γ_{hot}. Notably, apart from increasing γ_{hot}, increasing the heat transfer coefficient h_{hot} can also enhance the maximum power density output.

Next, a parametric study is conducted to optimize the RC-TE device. First, the effect of h_{cod} and h_{hot} is evaluated. During simulation, the testing condition is used and γ_{cold} is set as 250. As shown in Fig 5(a)-(b), the temperature difference and power density increase with increasing h_{hot} and decreasing h_{cod}. Thus, the best combination of h_{cod} and h_{hot} is that high h_{hot} and low h_{cod}. For example, the temperature difference and power density reach 3.6 K and 71.9 $mW \cdot m^{-2}$ when h_{cod} and h_{hot} are set as 0.01 and 20 $W \cdot m^{-2} \cdot K^{-1}$. The main reason for this phenomenon is that the ability to extract heat from ambient air is enhanced by increasing h_{hot} and net cooling power of the cooler is improved by decreasing h_{cold}, which simultaneously contributes to improving the performance of the RC-TE device. Second, Fig 5(c)-(d) depicts the temperature difference and power density of the RC-TE device under different ambient temperature and dew point temperature. Notably, h_{cold} and h_{hot} are changed to be 0.01 and 20 $W \cdot m^{-2} \cdot K^{-1}$ in the testing condition since this combination is the best one concluded from Fig. 5(a)-(b). Here, we introduce practical means by which one can improve the heat transfer processes at the cold and hot sides of the TEG. On the cold side, a wind cover, such as polyethylene film[3,15,49], can be used to reduce h_{cold}. To further reduce h_{cold} and keep the radiative cooling surface more stable in practical applications, a rigid infrared transparent window (for example, made from zinc selenide[50,51]) and a vacuum environment are desirable. On the hot side, using a thermally optimized heat sink can maximize heat transfer between the air and the thermoelectric generator.

Third, it is evident from Figure 5(c)-(d) that the best condition for the RC-TE device is when the ambient temperature is high and the dew point temperature is low. Thermodynamically, high ambient temperature and low dew point temperature means the atmosphere is very dry, which corresponds to a good sky condition for radiative cooling and thus improve the performance of the RC-TE device. The temperature difference and power density of the RC-TE device can be nearly 7.3 K and 291 mW·m^{-2} with ambient temperature and dew point temperature as 307.15 K and 283.15 K. Finally, we investigate the effect of P or N element's length L and area A on the performance of the RC-TE device. Following our determination of the best conditions for the RC-TE device obtained from the above analysis, h_{cold} and h_{hot} are set to be 0.01 and 20 W·m^{-2}·K^{-1}, and ambient temperature and dew point temperature are set to be 307.15 K and 283.15 K. Furthermore, we impose two further constraints. The one is that A changes within the constraint condition that the area fill factor of the PN thermocouples in the TEG module is within 0 to 1. The other is that the cold and hot side area ratio is maintained as a constant, i.e., $\gamma_{cold} = \gamma_{hot} = 250$. The results, shown in Fig. 5(e)-(f), reveal two important insights. On the one hand, temperature difference and power density of the RC-TE device is independent of A. The main reason for this result is that we keep the cold and hot area ratio at a constant, which means that the area of the cold and hot areas passively change with A, ultimately eliminating the effect A on the temperature difference and power density. On the other hand, there is an optimal power density achieved of the RC-TE device as a function of L. The above two results thus provide a reference for geometry optimization for the RC-TE device and the thermocouples used in the device.

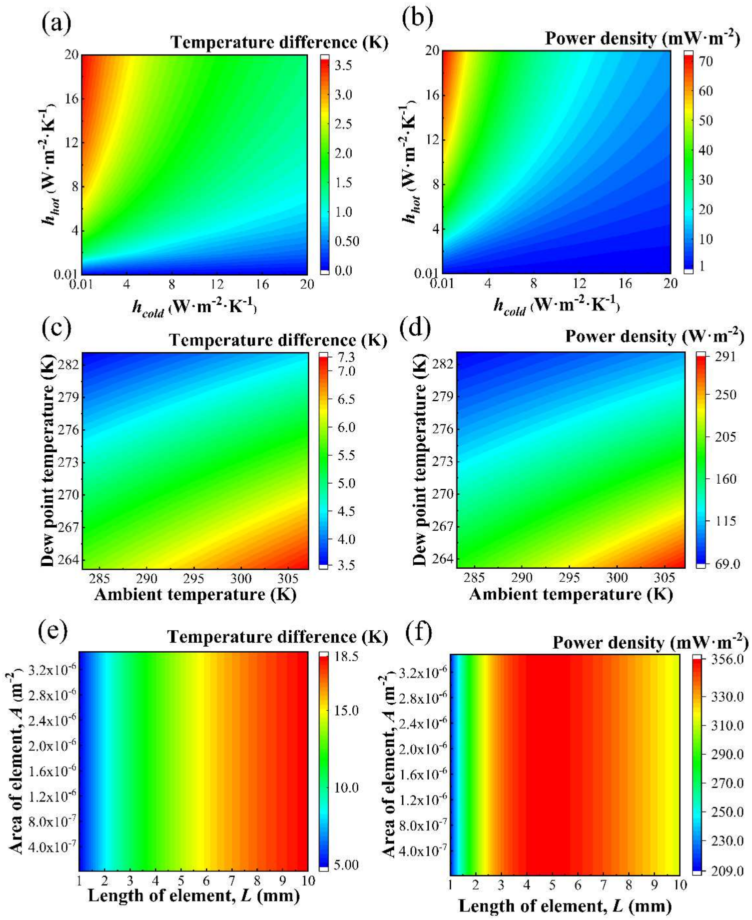

Fig. 5. (a)-(b)Temperature difference between the hot and cold side and power density of the RC-TE device under different h_{hot} and h_{cold}. (c)-(d) temperature difference between the hot and cold side and power density of the RC-TE device under different ambient temperature and dew point temperature. (e)-(f) temperature difference between the hot and cold side and power density of the RC-TE device under different length and area of P or N element.

To conclude, a theoretical model for the RC-TE device is developed and used to optimize its operating condition and geometry. The MPP and MEP obtained using the model in this work is different from that obtained by traditional TEG models, indicating the need to optimize for the operating condition of the RC-TE device differently than conventional approaches. Moreover, the area ratio between cooler and P or N element can be optimized to obtain a maximum power density of the device, which is an easily implementable means of optimizing the geometry of the RC-TE device. We next developed a parametric study that provides several further mechanisms to improve the performance of the RC-TE device, including enhancing heat transfer between the hot surface and ambient air, suppress the cooling loss of the cooler, dry atmosphere, and optimal length of the P or N element. In summary, this work provides universal guidance for RC-TE devices and identifies concrete pathways to optimize their performance. Given the potential importance of this class of energy harvesting device for night-time power generation applications, including lighting and low-power sensors, we hope that these results provide a practical pathway to maximizing their performance using materials and components widely available today.

Acknowledgments

This work has been supported by the National Natural Science Foundation of China (NSFC 51776193 and 51761145109) and a project funded by China Postdoctoral Science Foundation (2020TQ0307). A.P.R. acknowledges support of the Alfred P. Sloan Foundation, and the UCLA Hellman Fellows Award.

Data Availability Statement

The data that support the findings of this study are available from the corresponding author upon reasonable request.

References

[1] S. Fan and A. Raman, Natl. Sci. Rev. **5**, 132 (2018).

[2] B. Zhao, M. Hu, X. Ao, N. Chen, and G. Pei, Appl. Energy **236**, 489 (2019).

[3] Y. Zhai, Y. Ma, S.N. David, D. Zhao, R. Lou, G. Tan, R. Yang, and X. Yin, Science (80-.). **355**, 1062 (2017).

[4] C.G. Granqvist and A. Hjortsberg, Appl. Phys. Lett. **36**, 139 (1980).

[5] C.G. Granqvist and A. Hjortsberg, J. Appl. Phys. **52**, 4205 (1981).

[6] C.G. Granqvist, Appl. Opt. **20**, 2606 (1981).

[7] C.G. Granqvist, A. Hjortsberg, and T.S. Eriksson, Thin Solid Films **90**, 187 (1982).

[8] E.M. Lushiku, T.S. Eriksson, A. Hjortsberg, and C.G. Granqvist, Sol. Wind Technol. **1**, 115 (1984).

[9] A.W. Harrison and M.R. Walton, Sol. Energy **20**, 185 (1978).

[10] A. Hamza, I.M.S. Taha, and I.M. Ismail, Sol. Energy **55**, 235 (1995).

[11] M.D. Diatezua, P.A. Thiry, and R. Caudano, Vacuum **46**, 1121 (1995).

[12] M. Tazawa, P. Jin, and S. Tanemura, Thin Solid Films **281**, 232 (1996).

[13] S. Catalanotti, V. Cuomo, G. Piro, D. Ruggi, V. Silvestrini, and G. Troise, Sol. Energy **17**, 83 (1975).

[14] P. Grenier, Rev. Phys. Appl. **14**, 87 (1979).

[15] A.P. Raman, M.A. Anoma, L. Zhu, E. Rephaeli, and S. Fan, Nature **515**, 540 (2014).

[16] E. Rephaeli, A. Raman, and S. Fan, Nano Lett. **13**, 1457 (2013).

[17] X. Zhang, Science (80-.). **355**, 1023 (2017).

[18] T. Li, Y. Zhai, S. He, W. Gan, Z. Wei, M. Heidarinejad, D. Dalgo, R. Mi, X. Zhao, J. Song, J. Dai, C. Chen, A. Aili, A. Vellore, A. Martini, R. Yang, J. Srebric, X. Yin, and L. Hu, Science (80-.). **364**, 760 (2019).

[19] B. Zhao, M. Hu, X. Ao, N. Chen, Q. Xuan, Y. Su, and G. Pei, Energy **183**, 892 (2019).

[20] N. Fernandez, W. Wang, K. Alvine, and K. S, *Energy Savings Potential of Radiative Cooling Technologies* (2015).

[21] X. Lu, P. Xu, H. Wang, T. Yang, and J. Hou, Renew. Sustain. Energy Rev. **65**, 1079 (2016).

[22] D. Zhao, A. Aili, Y. Zhai, J. Lu, D. Kidd, G. Tan, X. Yin, and R. Yang, Joule **3**, 111 (2019).

[23] L. Zhu, A. Raman, K.X. Wang, M.A. Anoma, and S. Fan, Optica **1**, 32 (2014).

[24] L. Zhu, A.P. Raman, and S. Fan, Proc. Natl. Acad. Sci. **112**, 12282 (2015).

[25] B. Zhao, M. Hu, X. Ao, and G. Pei, Sol. Energy **176**, 248 (2018).

[26] Y. Lu, Z. Chen, L. Ai, X. Zhang, J. Zhang, J. Li, W. Wang, R. Tan, N. Dai, and W. Song, Sol. RRL **1**, 1700084 (2017).

[27] J.K. Tong, X. Huang, S. V. Boriskina, J. Loomis, Y. Xu, and G. Chen, ACS Photonics **2**, 769 (2015).

[28] P.-C. Hsu, A.Y. Song, P.B. Catrysse, C. Liu, Y. Peng, J. Xie, S. Fan, and Y. Cui, Science (80-.). **353**, 1019 (2016).

[29] L. Cai, A.Y. Song, W. Li, P.-C. Hsu, D. Lin, P.B. Catrysse, Y. Liu, Y. Peng, J. Chen, H. Wang, J. Xu, A. Yang, S. Fan, and Y. Cui, Adv. Mater. **30**, 1802152 (2018).

[30] L. Cai, A.Y. Song, P. Wu, P.C. Hsu, Y. Peng, J. Chen, C. Liu, P.B. Catrysse, Y. Liu, A. Yang, C. Zhou, C. Zhou, S. Fan, and Y. Cui, Nat. Commun. **8**, 496 (2017).

[31] P.-C. Hsu, C. Liu, A.Y. Song, Z. Zhang, Y. Peng, J. Xie, K. Liu, C.-L. Wu, P.B. Catrysse, L. Cai, S. Zhai, A. Majumdar, S. Fan, and Y. Cui, Sci. Adv. **3**, e1700895 (2017).

[32] S.J. Byrnes, R. Blanchard, and F. Capasso, Proc. Natl. Acad. Sci. **111**, 3927 (2014).

[33] S. Buddhiraju, P. Santhanam, and S. Fan, Proc. Natl. Acad. Sci. U. S. A. **115**, E3609 (2018).

[34] W. Li, S. Buddhiraju, and S. Fan, Light Sci. Appl. **9**, 68 (2020).

[35] M. Ono, P. Santhanam, W. Li, B. Zhao, and S. Fan, Appl. Phys. Lett. **114**, 161102 (2019).

[36] A.P. Raman, W. Li, and S. Fan, Joule **3**, 2679 (2019).

[37] S. Ishii, T.D. Dao, and T. Nagao, Appl. Phys. Lett. **117**, 013901 (2020).

[38] E. Mu, Z. Wu, Z. Wu, X. Chen, Y. Liu, X. Fu, and Z. Hu, Nano Energy **55**, 494 (2019).

[39] Z. Xia, Z. Zhang, Z. Meng, L. Ding, and Z. Yu, ACS Appl. Mater. Interfaces **11**, 33941 (2019).

[40] D. Kraemer, B. Poudel, H.-P. Feng, J.C. Caylor, B. Yu, X. Yan, Y. Ma, X. Wang, D. Wang, A. Muto, K. McEnaney, M. Chiesa, Z. Ren, and G. Chen, Nat. Mater. **10**, 532 (2011).

[41] A. Yamada, Japan patent JPB 002716861 (1997).

[42] L. Fan, W. Li, W. Jin, M. Orenstein, and S. Fan, Opt. Express **28**, 25460 (2020).

[43] G. Chen, J. Appl. Phys. **109**, 104908 (2011).

[44] W. He, G. Zhang, G. Li, and J. Ji, Energy Convers. Manag. **98**, 268 (2015).

[45] G. Li, K. Zhou, Z. Song, X. Zhao, and J. Ji, Energy Convers. Manag. **161**, 155 (2018).

[46] M. Gomez, R. Reid, B. Ohara, and H. Lee, J. Appl. Phys. **113**, 174908 (2013).

[47] G. Li, X. Zhao, and J. Ji, Energy Convers. Manag. **126**, 935 (2016).

[48] P. Berdahl and R. Fromberg, Sol. Energy **29**, 299 (1982).

[49] W. Li, Y. Shi, Z. Chen, and S. Fan, Nat. Commun. **9**, 4240 (2018).

[50] Z. Chen, L. Zhu, A. Raman, and S. Fan, Nat. Commun. **7**, 13729 (2016).

[51] Z. Chen, L. Zhu, W. Li, and S. Fan, Joule 1 (2018).

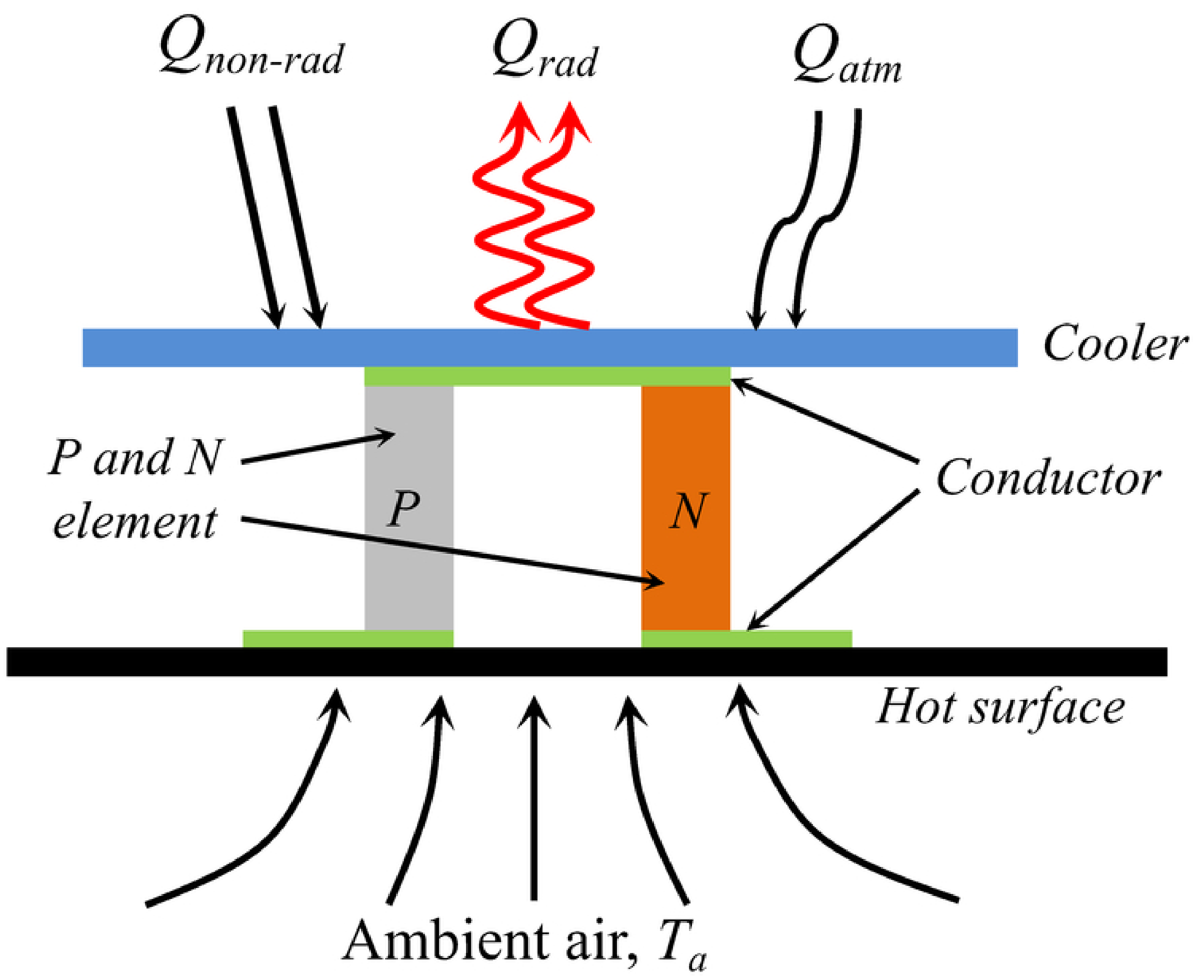
$Q_{non\text{-}rad}$
Q_{rad}
Q_{atm}
Cooler
P and N element
P
N
Conductor
Hot surface
Ambient air, T_a

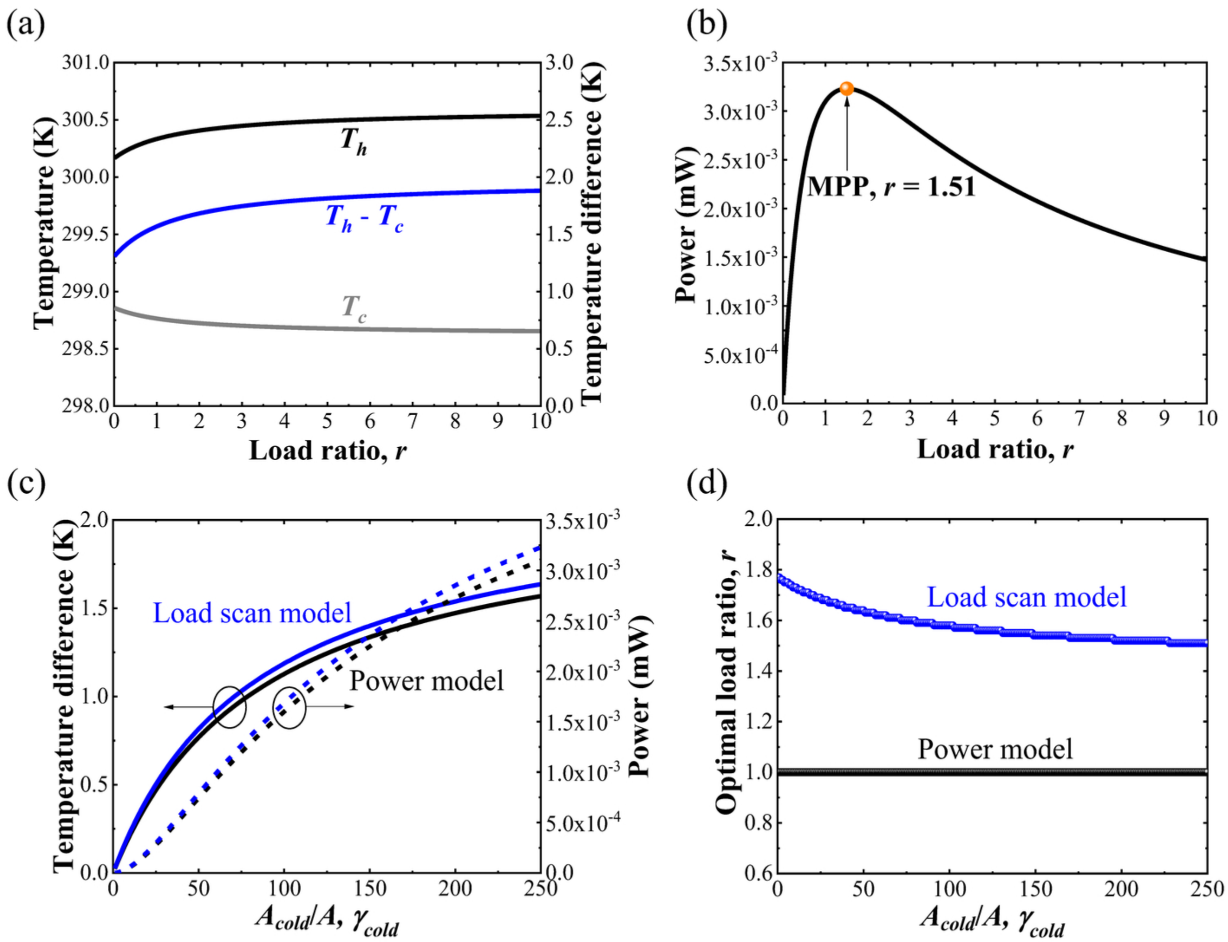
(a)
Temperature (K)
Temperature difference (K)
T_h
T_h - T_c
T_c
Load ratio, r
(b)
Power (mW)
MPP, r = 1.51
Load ratio, r
(c)
Temperature difference (K)
Power (mW)
Load scan model
Power model
A_{cold}/A, γ_{cold}
(d)
Optimal load ratio, r
Load scan model
Power model
A_{cold}/A, γ_{cold}

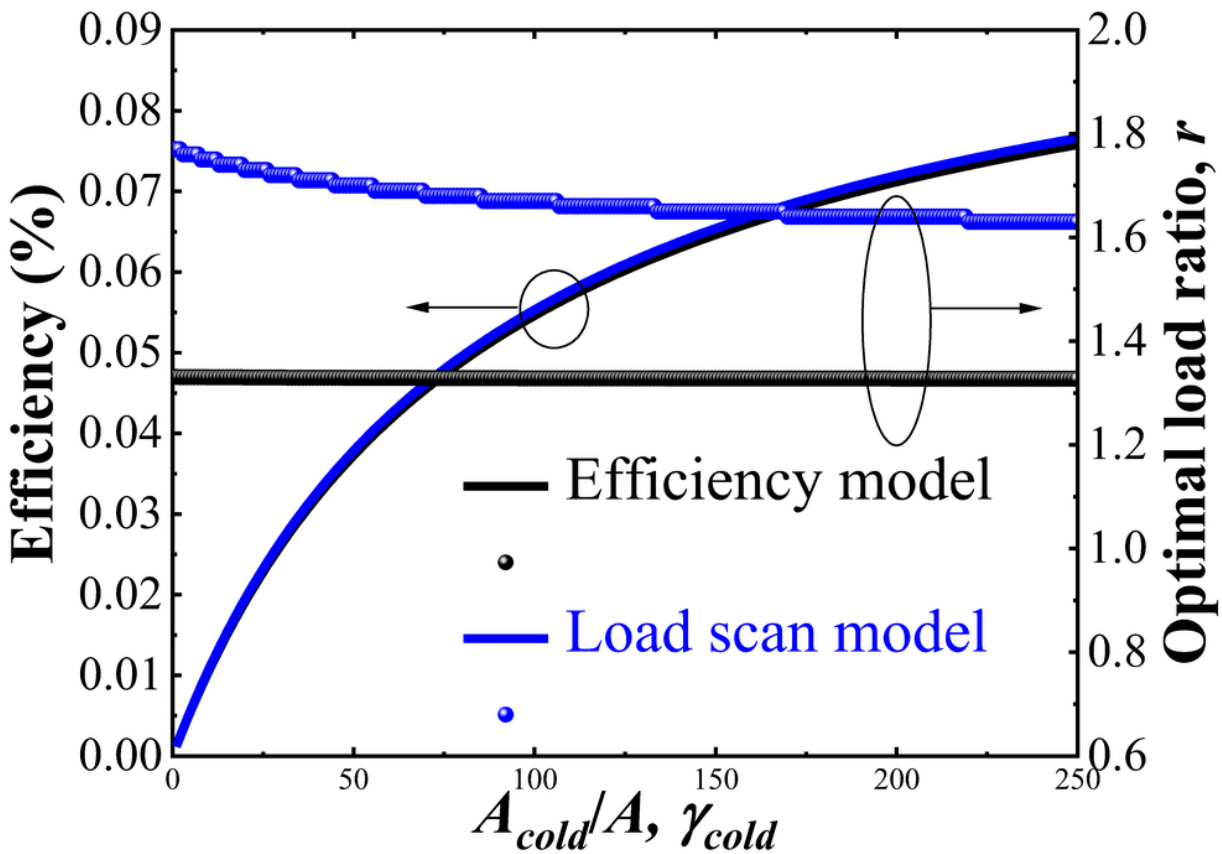
Efficiency (%)
Optimal load ratio, r
A_{cold}/A, γ_{cold}
Efficiency model
Load scan model
0.00
0.01
0.02
0.03
0.04
0.05
0.06
0.07
0.08
0.09
0.6
0.8
1.0
1.2
1.4
1.6
1.8
2.0
0
50
100
150
200
250

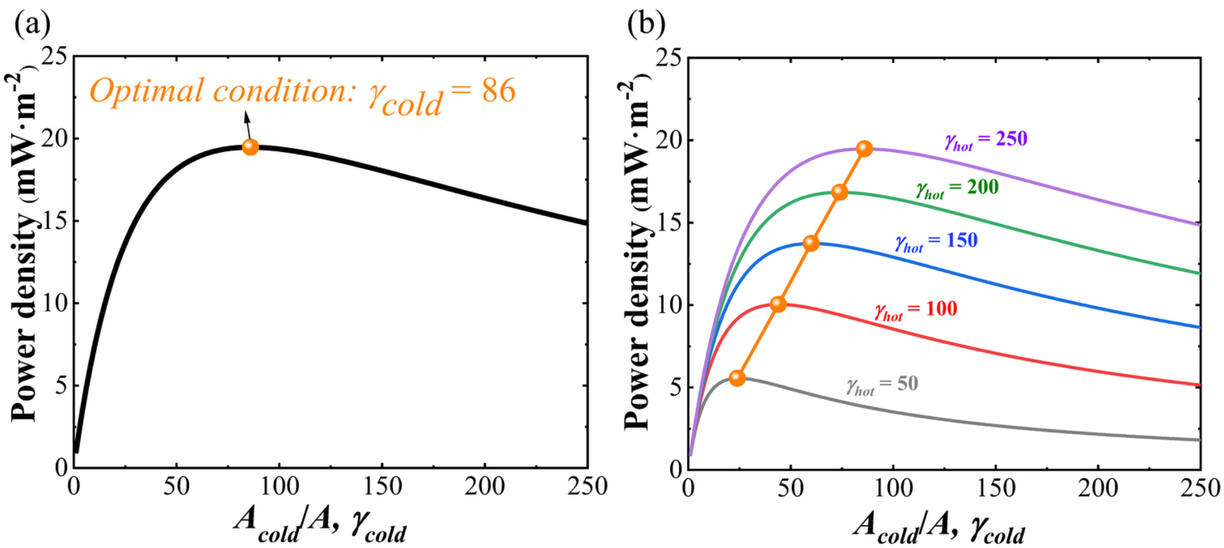
(a)
Optimal condition: γcold = 86
Power density (mW·m-2)
Acold/A, γcold
(b)
γhot = 250
γhot = 200
γhot = 150
γhot = 100
γhot = 50
Power density (mW·m-2)
Acold/A, γcold

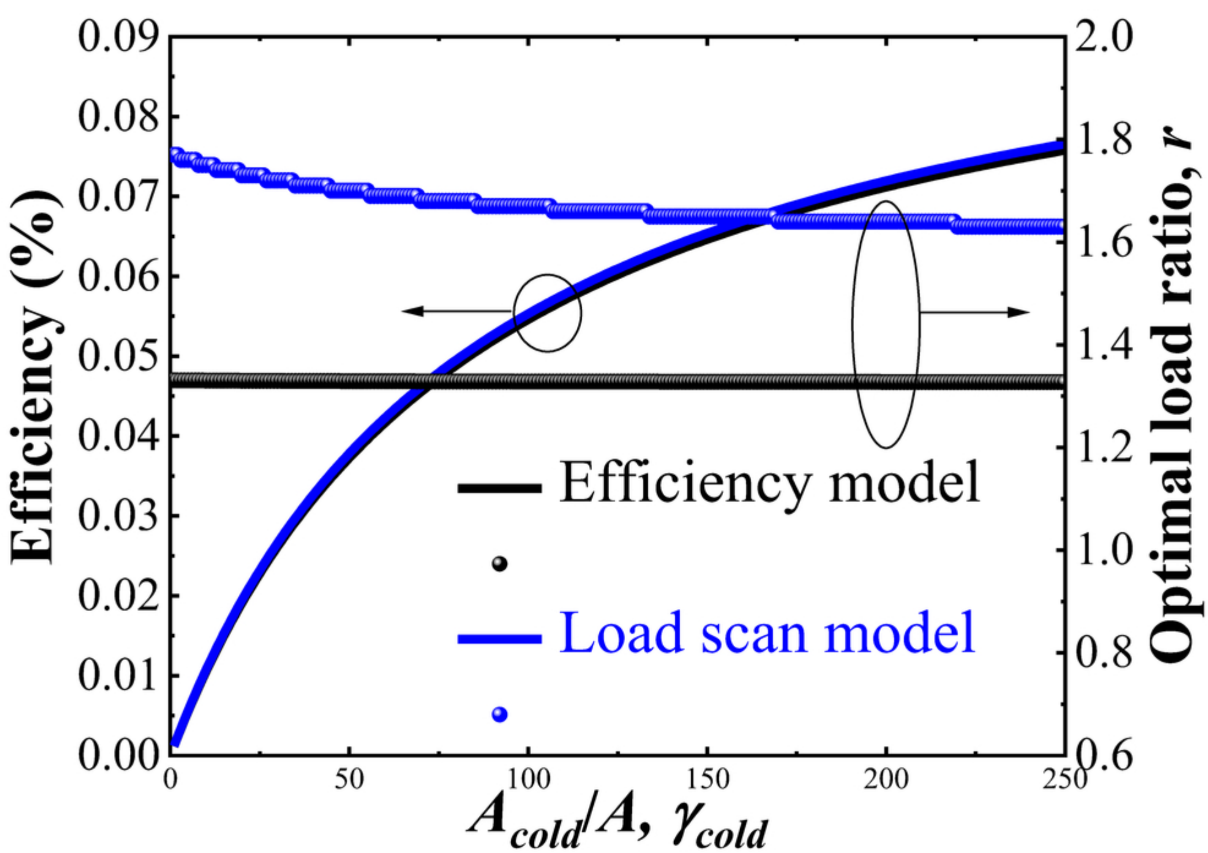
Efficiency (%)
Optimal load ratio, r
A_{cold}/A, γ_{cold}
Efficiency model
Load scan model
0.00
0.01
0.02
0.03
0.04
0.05
0.06
0.07
0.08
0.09
0.6
0.8
1.0
1.2
1.4
1.6
1.8
2.0
0
50
100
150
200
250

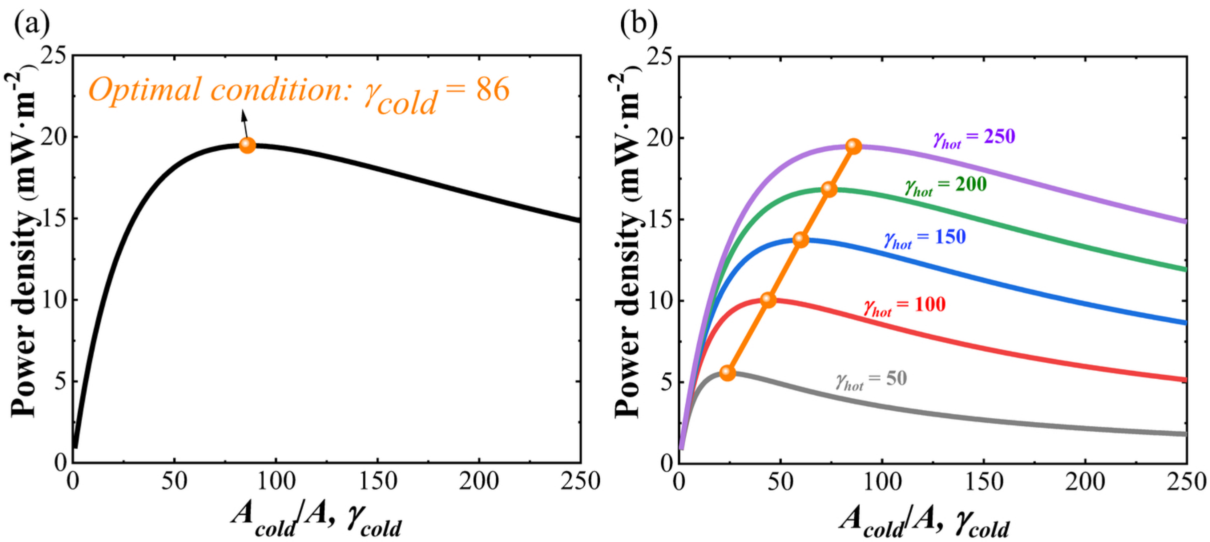
(a)
Optimal condition: γ_{cold} = 86
Power density (mW·m^{-2})
A_{cold}/A, γ_{cold}
0
5
10
15
20
25
50
100
150
200
250
(b)
γ_{hot} = 250
γ_{hot} = 200
γ_{hot} = 150
γ_{hot} = 100
γ_{hot} = 50
Power density (mW·m^{-2})
A_{cold}/A, γ_{cold}

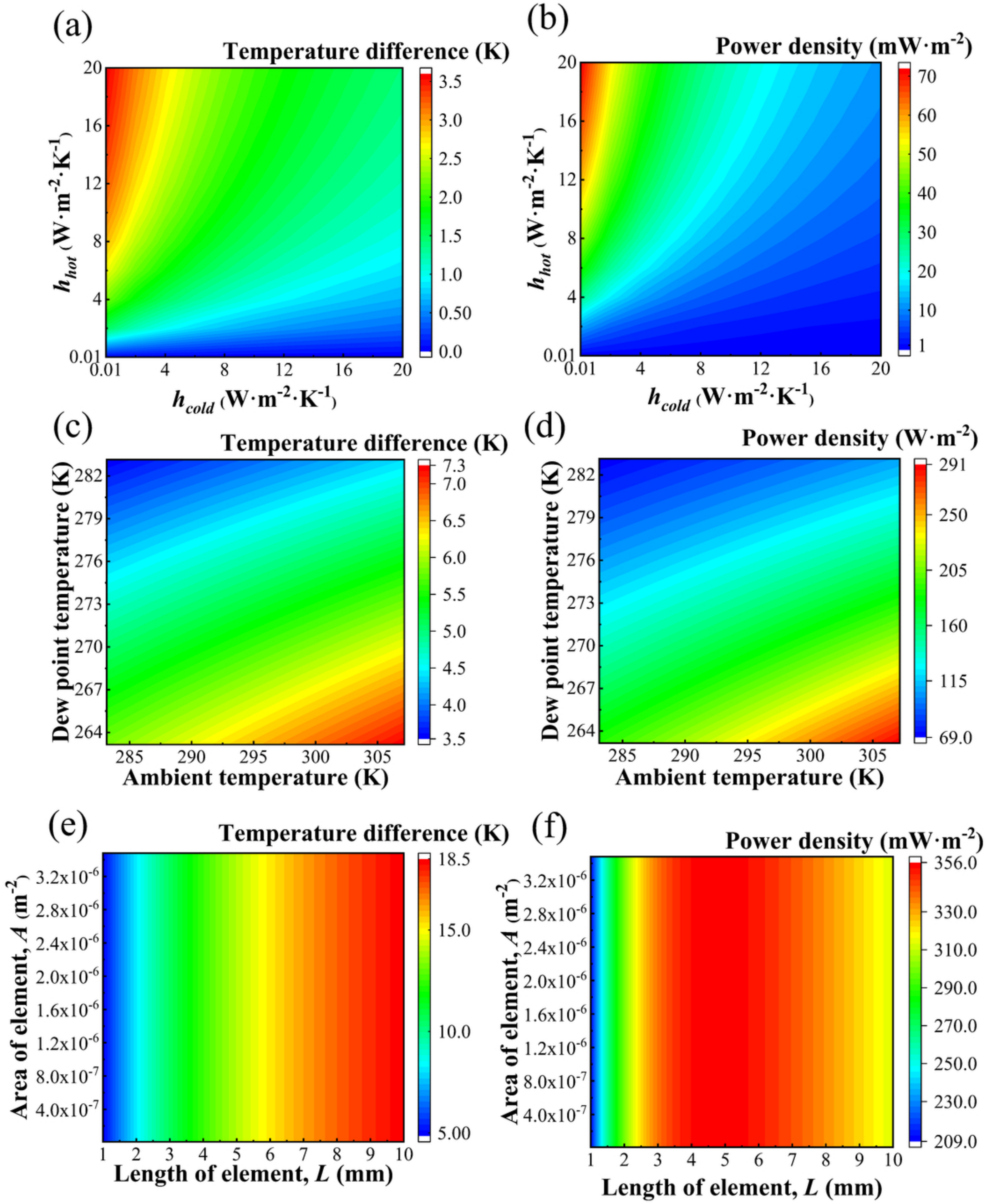
(a)
Temperature difference (K)
h_hot (W·m^-2·K^-1)
h_cold (W·m^-2·K^-1)
(b)
Power density (mW·m^-2)
h_hot (W·m^-2·K^-1)
h_cold (W·m^-2·K^-1)
(c)
Temperature difference (K)
Dew point temperature (K)
Ambient temperature (K)
(d)
Power density (W·m^-2)
Dew point temperature (K)
Ambient temperature (K)
(e)
Temperature difference (K)
Area of element, A (m^-2)
Length of element, L (mm)
(f)
Power density (mW·m^-2)
Area of element, A (m^-2)
Length of element, L (mm)